Structure and Raman Spectrum of Clavulanic Acid in Aqueous Solution

ARTICLE *in* THE JOURNAL OF PHYSICAL CHEMISTRY B · APRIL 2007

Impact Factor: 3.3 · DOI: 10.1021/jp066135u · Source: PubMed

4 AUTHORS, INCLUDING:

Simone Raugei
Pacific Northwest National Laboratory
96 PUBLICATIONS **1,742** CITATIONS
SEE PROFILE

Paolo Carloni
Forschungszentrum Jülich
320 PUBLICATIONS **6,082** CITATIONS
SEE PROFILE

Marion S Helfand
Louis Stokes Cleveland VA Medical Center
56 PUBLICATIONS **1,211** CITATIONS
SEE PROFILE

Structure and Raman Spectrum of Clavulanic Acid in Aqueous Solution

Andrea Miani,[†] Simone Raugei,*[,†] Paolo Carloni,[†] and Marion S. Helfand[‡]

SISSA/ISAS and INFM-DEMOCRITOS, Modeling Center for Research in Atomistic Simulation, via Beirut 2, I-34014, Trieste, Italy, and Case School of Medicine, Louis Stokes, Cleveland Department of Veterans Affairs Medical Center, Departments of Medicine and Biochemistry, Case Western Reserve University, Cleveland, Ohio 44106

Received: September 19, 2006; In Final Form: December 5, 2006

The calculation of the vibrational Raman spectrum of enzyme-bound β-lactamase inhibitors may be of help to understand the mechanisms responsible for bacterial drug resistance. Here, we present a study of the solvation structure and the vibrational properties of clavulanate, an imporant β-lactamase inhibitor, in aqueous solution as obtained from full quantum and hybrid empirical/quantum molecular dynamics simulations at ambient conditions. The analysis of the vibrational density of states indicates that hybrid empirical/quantum mechanical simulations are able to properly describe the vibrational levels of clavulanate in solution. In addition, we propose a computationally efficient protocol to calculate the vibrational Raman effect for large solute molecules in water, which is able to faithfully reproduce the experimentally recorded clavulanate Raman spectrum and discloses the possibility to employ hybrid simulations to assign the experimental Raman spectra of inhibitors bound to β-lactamases.

1. Introduction

Bacterial resistance to antibiotics mediated by β-lactamases is a major clinical problem worldwide. β-lactamase inhibitors are usually employed to enhance the therapeutic efficacy of specific antibiotics, but several aspects of the involved reactions are still to be understood (ref 1 and references therein). In this respect, single-crystal Raman[2] microscopy revealed itself as a powerful tool to follow the chemical activity of β-lactamases, particularly of SHV-1 β-lactamase with tazobactam, sulbactam, and clavulanic acid,[1,3−5] the only three inhibitors of class A β-lactamase enzymes that are clinically available at the moment.[6] Indeed Raman microscopy allows one to identify intermediates, to follow the reaction pathway, and to measure the accumulation and decay rates for all of the reactive species involved in the process. These studies may help understand the mechanisms responsible for bacterial drug resistance and for developing new effective inhibitors through rational drug design.

The interpretation of the Raman spectra crucially depends on the assignment of the spectral experimental features. Computational methods can nowadays be proficiently employed in order to interpret spectral experimental data. During the last years, considerable progress has been made in the calculation from first principles of vibrational spectra of polyatomic molecules. The vibrational levels of small three- and four-atom isolated molecules can nowadays be calculated without any empirical parameter or scaling factor within 1 cm^{-1}.[7,8] For larger molecular systems, the average maximum obtainable accuracy is approximatively 10/20 cm^{-1}.[9−11] These calculations solve either variationally or perturbatively the Schrödinger equation for the atomic nuclei, employing analytic expressions for the potential energy surfaces (PESs) obtained from highly accurate *ab initio* methods. For large solvated systems, this approach cannot obviously be employed, but nevertheless accurate results have been obtained from direct *ab initio* simulations:[12,13] atomic nuclei are treated classically, the system evolves following the Newton equations of motion, and the intra- and intermolecular potential is provided by the *ab initio* PES, which is calculated on the fly. The structure and the dynamical properties of the system, such as the vibrational density of states (VDOS), together with the infrared[14−19] and Raman[20,21] spectral information can be then, in principle, computed from the classic trajectory of motion. Mixed quantum mechanical-molecular mechanical methods (QM/MM) can then be employed to extend the capabilities of current computational techniques to systems made of thousands of atoms. QM/MM simulations, in particular, have been employed in the calculation of infrared spectra of complex solvated systems of biological relevance, taking fully into account the anharmonicity of the PES at finite temperature.[15,19,22−27] In contrast, to the best of our knowledge, no QM/MM calculations of Raman spectra of biological systems have been reported so far.

Here, we calculate the structure, the vibrational properties and Raman spectrum of clavulanate (Figure 1a) in aqueous solution by means of direct full *ab initio* (Car−Parrinello) simulations and compare these to the results obtained by hybrid QM/MM,[13,28,29] in which clavulanate is treated quantum mechanically and water by means of molecular mechanics (MD). The main difficulty lies in the calculation of the polarizability tensor of the system. Recently, methods to calculate the dielectric tensor in the linear response regime within a plane-wave density functional theory (DFT) scheme has been proposed[20,30] and applied to the study of the Raman spectrum of ice in different crystalline phases,[21] zeolites,[30] and BN nanotubes.[31] This approach is however computationally demanding to be used routinely with *ab initio* MD simulations of large systems. Herein, we propose an alternative simple protocol to calculate the vibrational Raman effect. Briefly, we sample the relevant phase space of the system via QM/MM simulations; then, on configurations equispaced in time we calculate the

[†] SISSA/ISAS and INFM-DEMOCRITOS.
[‡] Case School of Medicine.

10.1021/jp066135u CCC: $37.00
Published on Web 02/16/2007

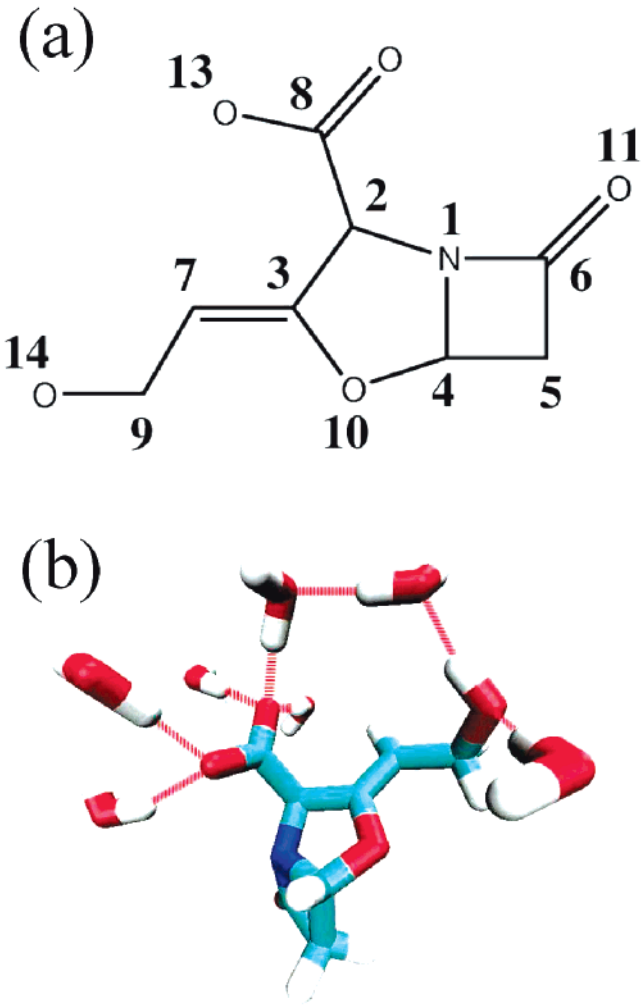

Figure 1. (a) Clavulanate structure along with the labeling of the heavy atoms employed in this work; (b) Average solvation structure of clavulanate in aqueous solution as obtained from the QM simulation.

molecular polarizability tensor of clavulanate in the presence of the solvent electrostatic fields using computationally efficient standard quantum mechanical approaches. In this way, we were able to reproduce and interpret the main spectral features of the experimental vibrational Raman spectrum of clavulanate in solution.

The paper is organized as follows. In Section 2, the computational details are given. In particular, in Section 2.2, we extensively explain the computational protocol used to calculate the Raman activity. Then, we discuss the structural data (Section 3.1) and the vibrational properties (Section 3.2) of clavulanate in water. Finally, we report and interpret the calculated Raman spectrum in Section 3.3. The main results are summarized and commented on in Section 4.

2. Computational Methods

2.1. Electronic Structure Calculations and Molecular Dynamics Simulations. Clavulanic acid in aqueous solution is present mostly as clavulanate. Therefore, we first ran a classical molecular dynamics simulation of clavulanate in TIP3P[32] water at constant atmospheric pressure and at room temperature using the Amber package.[33] The clavulanate force field has been parametrized using the General Amber Force Field (GAFF),[34] whereas the Restrained ElectroStatic Potential fit (RESP) charges have been obtained with the MOPAC semiempirical method available with Antechamber.[35] We chose to work in the infinite dilution limit. Clavulanate was immersed in an orthorhombic box containing about 800 TIP3P water molecules and equilibrated for 1.0 ns. The simulation was then continued for 5.0 ns at constant volume at the calculated average density employing a Langevin thermostat at 300 K.[36] Because this simulation was performed to have a good initial configuration for the subsequent QM and QM/MM simulations, we did not include a counterion to balance the negative charge of the molecule to avoid strong finite size effects. Instead, a positive neutralizing background was added.

Starting from a snapshot of the second classical MD simulation, a constant volume hybrid Quantum Mechanics−Car−Parrinello (CP)/Molecular Mechanics[12,13,28,29] simulation was performed at room temperature partitioning the system into a quantum part (clavulanate) and a classical part (TIP3P water). The quantum region was described within gradient-corrected DFT using the Becke[37] and Lee, Yang, and Parr[38] (BLYP) exchange and correlation energy functionals. Norm-conserving Martins−Troullier pseudopotentials[39] were used to describe the interactions between the core and valence electrons for all atoms but for hydrogens, for which a Von Bart−Car-type pseudopotential[40,41] was used to smooth out the short-range Coulombic nuclear potential. The Kohn−Sham orbitals of valence electrons were expanded in plane waves with kinetic energy up to 70 Ry. The electrostatic coupling between the QM and the MM region is calculated by using the full Hamiltonian scheme proposed by Rothlisberger and co-workers[28,29] as implemented in the CP code CPMD3.5.[42] Explicit electrostatic interactions between clavulanate and water were taken into account within 5.3 Å of clavulanate, whereas the interaction between dynamically fitted D-RESP point charges[29] centered on the QM atoms and RESP[43] charges on the MM were considered for MM atoms between 5.3 and 10.6 Å of clavulanate. Electrostatic interactions between the MM atoms and a multipole expansion[28] representing the charge distribution of the QM region was considered for MM atoms beyond 10.6 Å. The Car−Parrinello equations of motions were integrated using a fictitious electronic mass of 600 au and a time-step of 0.12 fs. The system was equilibrated for 1 ps; then, the trajectory was sampled for 9.74 ps. During the equilibration, the temperature was kept at 300 K employing a Nose−Hoover chain of thermostats.[44]

From the constant volume classical simulation, a constant volume CP MD simulation where both clavulanate and water were treated at the quantum level was also performed. To this end, a smaller box was used in order to make the size of the system manageable. The simulation box was chosen in a such a way to retain the first two clavulanate solvation shells and the average density inferred from the classical simulation. In this way, 61 water molecules in a 12.75 Å-side box were explicitly considered. This simulation box was reequilibrated at constant temperature first with a classical MD run and then with a 1 ps-long CP MD run at 300 K. After equilibration, the CP MD trajectory was collected for 10.35 ps.

Gas phase geometry optimization and vibrational analysis of clavulanate were also performed using both the CPMD program[42] and the Gaussian03 package.[45] For the CPMD calculations, we used the same DFT setup employed in the MD simulations enclosing the molecule in an empty periodic box (12.75 Å) and using the electrostatic decoupling scheme proposed in ref 46. For the Gaussian calculation, we optimized the structure of clavulanate using both the BLYP[37,38] and the B3LYP[47] functionals along with the cc-pVDZ and the cc-pVTZ basis sets.[48] These calculations allow us to validate the use of norm-conserving pseudopotentials for the analysis of vibra-

tional properties and the assessment of the finite temperature and solvent effects on the vibrational properties and on the Raman spectrum. The cubic and semidiagonal quartic force constants have been then calculated using the B3LYP and the cc-pVDZ basis set; with these, the second order anharmonic corrections to the harmonic fundamentals for clavulanate have been calculated and are reported in Table 4. The fundamental vibrational modes have been determined using the equation:

$$\nu_i = \omega_i + 2x_{i,i} + \frac{1}{2}\sum_{j\neq i} x_{i,j} \quad (1)$$

where ω_i is the harmonic frequency and the $x_{i,j}$ values are the second order anharmonic constants, whose expression as a function of the harmonic, cubic, and semi-diagonal quartic force constants, and the equilibrium rotational constants, is reported, for example, in ref 49.

Finally, to evaluate the solvation effects both on the molecular structure and on the vibrational density of states of the system, we compare the results of the simulations in solution with those of a CPMD simulation in the gas phase at room temperature. For this simulation, the previously described setup and MD protocol were used. We also analyzed the microsolvation effect on the clavulanate Raman spectrum calculating the harmonic frequencies and the Raman intensities for an average configuration obtained from the QM simulation, which includes all of the water molecules (seven) forming hydrogen bonds with the oxygens in clavulanate (Figure 1b).

2.2. Calculation of the Raman Activity. The vibrational Raman activity was calculated both via standard quantum chemistry and via a QM/MM protocol as described in the ensuing paragraphs.

2.2.1. Standard Quantum Chemistry Approach. The gas phase Raman scattering activity has been obtained using the expressions:[50]

$$I_\perp = 45\alpha'^2 + 7\beta'^2 \quad (2)$$

where $I_\perp$ refers to the total Raman scattering activity determined by the perpendicular component of the incident light electric field with respect to the scattering direction. The terms α' and β' appearing in $I_\perp$ are defined as:

$$\alpha' = \frac{1}{3}(\alpha'_{x,x} + \alpha'_{y,y} + \alpha'_{y,y}) \quad (3)$$

and

$$\beta'^2 = \frac{1}{2}[(\alpha'_{x,x} - \alpha'_{y,y})^2 + (\alpha'_{x,x} - \alpha'_{z,z})^2 + (\alpha'_{y,y} - \alpha'_{z,z})^2 + 6(\alpha'^2_{x,y} + \alpha'^2_{x,z} + \alpha'^2_{y,z})] \quad (4)$$

where the prime indicates the derivative of the polarizability tensor elements with respect to the normal modes.[51,52] The first derivatives of the polarizability tensor have been calculated by finite differences displacing the molecule along its linear normal coordinates calculated at equilibrium. To calculate the relative Raman cross sections for the harmonic frequencies, the Raman scattering activity has been corrected with the factor

$$I = \frac{I_\perp}{\nu_i[\exp(h\nu_i/k_B T) - 1]} \quad (5)$$

where h is the Planck constant, k_B is the Boltzmann constant, and T is the absolute temperature.

2.2.2. Raman Spectrum in Aqueous Solution: a QM/MM Protocol. The Raman spectrum of a solute in aqueous solution can be calculated from the ensemble averaged time autocorrelator of the dielectric tensor in the laboratory-based Cartesian frame that identifies the vector of the incident light.[53] All of the molecules of the solution contribute to the dielectric tensor, but because the Raman spectrum of water is weak and unobtrusive in the spectral region of interest, it is possible to neglect any direct water contribution to the Raman spectrum and focus on the solute polarizability tensor only.

To make a connection with experiments,[50] we have looked at the Raman effect due to the perpendicular component of the incident light electric field with respect to the scattering direction. For spatially isotropic systems such as aqueous solutions, it possible to average over all of the equivalent directions of the incident light. In this way, the following expression for the Raman scattering cross section per unit of solid angle and unit of frequency, $I_\perp(\omega)$, observed perpendicularly to the incident light of frequency ω_0 can be written:[54,53]

$$I_\perp(\omega) \propto \frac{1}{2\pi}(\omega_0 - \omega)^4 \int \mathrm{d}t\, \mathrm{e}^{-i\omega t} \langle \mathrm{Tr}\beta(0)\,\beta(t)\rangle^+_{qm} = \frac{1}{2\pi}(\omega_0 - \omega)^4 C_{qm}(\omega) \quad (6)$$

where β is a traceless anisotropic part of clavulanate polarizability α calculated in a molecular fixed frame, $\beta = \alpha - \bar{\alpha}\mathbf{I}$ ($\bar{\alpha}$ is the average of the polarizability tensor trace and $\mathbf{I}$ is the unit tensor). Following Bader and Berne,[55] we approximate the Fourier transform of the symmetrized quantum mechanical autocorrelation function, $C_{qm}(\omega)$, in terms of the corresponding classical autocorrelation function, $C_{cl}(t)$, as

$$C_{qm}(\omega) = \frac{\hbar\omega}{2k_B T}\coth\left(\frac{\hbar\omega}{2k_B T}\right) C_{cl}(\omega) \quad (7)$$

where $\hbar$ is the reduced Planck constant.

Employing the trajectory obtained from the QM/MM simulation, the time evolution of the polarizability tensor has been followed by extracting one configuration every 3.6 fs. The polarizability tensor for the chosen molecular configurations has been then calculated using both the BLYP and B3LYP exchange and correlation functionals with the basis set cc-pVTZ. In the calculation, the effects of the solvent were explicitly considered including the electrostatic potential[56,57] due to a spherical shell of TIP3P water molecules as obtained from the QM/MM trajectory. The calculation of the polarizability tensor for every snapshot took about 25 min on average with the B3LYP functional and 17 min with the BLYP functional on an IBM SP5 single processor. We tested that the used number of water molecules was large enough to have converged values of the polarizability tensor. The variation of the isotropic part of the polarizability tensor calculated at a given configuration as a function of the number of water molecules is shown in Figure 2. It can be seen that, from an initial value of 120 Bohr^3, the value of the polarizability tensor trace converges to 110.7 Bohr^3 when the second shell of water molecules is included and remains constant as the number of water molecules is increased. A similar behavior is observed for all the nine components of the polarizability and for different configurations randomly taken along the trajectory. We thus decided not to include in the calculation of the polarizability any water molecule belonging to the main box's periodic images.

It is of some interest to analyze the change of clavulate's polarizability going from the gas phase to the aqueous solution.

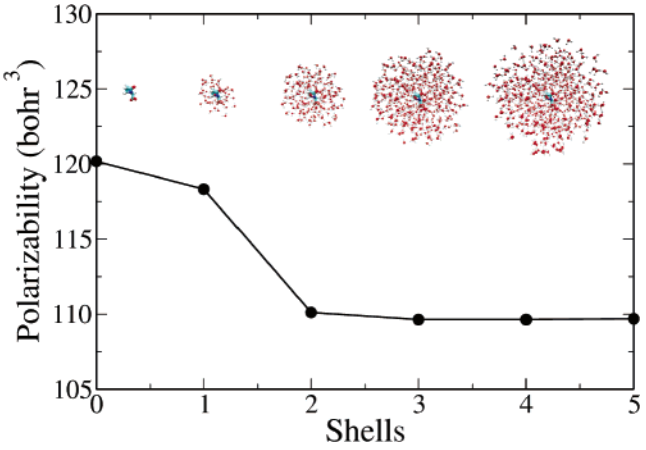

Figure 2. Variation of the isotropic polarizability of clavulanate as a function of the solvation shell diameter. The configuration has been taken from the calculated QM/MM trajectory.

TABLE 1: Average Values (in Bohrs^3) for the Principal Components of the Polarizability Tensor Obtained from the QM/MM Simulation of Solvated Clavulanate Compared with the Values Obtained for the Optimized Structure of the Isolated Molecule[a]

	BLYP isolated	B3LYP isolated	BLYP QM/MM	B3LYP QM/MM
α_1	158.2	143.0	135.3 (4.4)	130.2 (4.2)
α_2	128.7	115.8	102.9 (0.6)	98.7 (2.1)
α_3	103.5	98.9	86.1 (3.2)	84.0 (3.1)

[a] Standard deviations from the average are given in parantheses.

The average values for the principal components of the polarizability tensor for solvated clavulanate along with the values obtained at the equilibrium configuration for the isolated molecule are reported in Table 1. It can be seen that the variation of the polarizability components calculated at the equilibrium configuration for the isolated molecule when compared to the solvated systems decrease in average of the 17.1% for the BLYP and the 12.9% for the B3LYP calculations, respectively.

3. Results and Discussion

3.1. Clavulanate Structure in the Gas Phase and in Solution. With the dual goal of evaluating the solvation effects on both structure and vibrational properties and understanding the relevance of anharmonicity, we start discussing the equilibrium structure of clavulanate in vacuo at 0 K and at room temperature (the optimized molecular structure in vacuo and the numbering of the heavy atoms is reported in Figure 1).

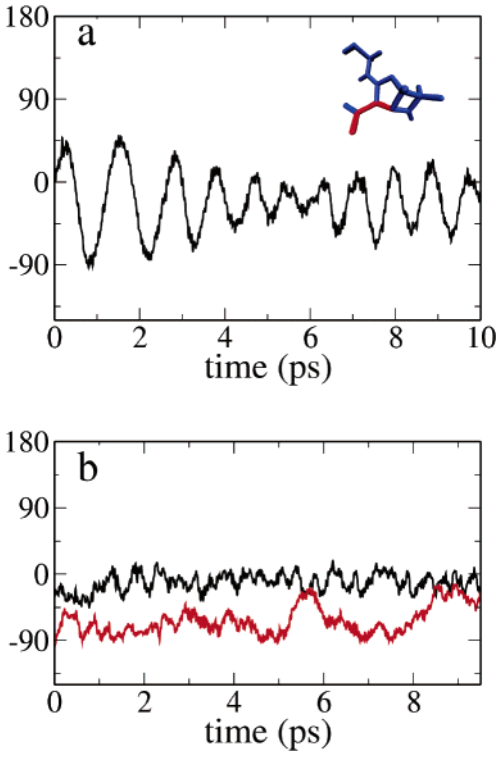

Figure 3. Gas phase (a) and solvated QM (b, black line) and QM/MM (b, red line) instantaneous value (in degrees) for the torsional angle $\tau_{1,2,8,12}$ defining the carboxylate orientation. The torsional angle is evidenced in red in the picture.

As one would expect, the flexible hydroxymethyl chain is largely affected by temperature (Table 2). Both the bending angle $\alpha_{7,9,14}$ and the torsional angles $\tau_{7,9,14,H}$ and $\tau_{3,7,9,14}$, which are connected to the hydroxymethyl group orientation, shift of 20.4°, 32.3°, and 109.9°, respectively. The instantaneous values obtained at 300 K in the gas phase for the torsional angle $\tau_{1,2,8,12}$, which describes the orientation of the carboxylate, oscillates almost periodically between −70° and 0° (Figure 3); the hydroxymethyl group (angle $\tau_{7,9,14,H}$) is allowed to move between about −50° and +50° (Figure 4). In solution, $\tau_{7,9,14,H}$ is not able to move as freely and similarly $\tau_{3,7,9,14}$ is hindered and the relative short simulation time does not allow us to see any conversion. The clavulanate structures as obtained from the QM and the QM/MM simulations in solution differ only in the $\tau_{1,2,8,12}$ torsional angle, which is related to the carboxylate group orientation. Both the QM and the QM/MM simulations seem to converge to a value for the torsional angle close to 0°, even

TABLE 2: Comparison between Selected Bond Lengths (in Ångstroms), Valence Angles (in Degrees), and Torsional Angles (in Degrees) Optimized with the BLYP Density Functional at 0 K, Calculated at 300 K in Vacuo and in Solution for Clavulanate[a]

	gas phase				solution/300K		
	0 K[b]	0 K[c]	0 K[d]	300 K[e]	Amber	QM	QM/MM
$r_{8,12}$	1.250	1.258	1.260	1.26[f]	1.22 (0.02)	1.28 (0.02)	1.28 (0.02)
$r_{8,13}$	1.245	1.255	1.259	1.26[f]	1.22 (0.02)	1.27 (0.02)	1.27 (0.02)
$r_{6,11}$	1.209	1.216	1.221	1.22[f]	1.22 (0.02)	1.22 (0.02)	1.22 (0.02)
$r_{14,H}$	0.967	0.973	0.975	0.98[f]	0.97 (0.01)	1.00 (0.02)	1.00 (0.03)
$\alpha_{9,14,H}$	106.2	106.3	106.5	105 (5)	106 (4)	107 (5)	106 (4)
$\alpha_{7,9,14}$	109.9	109.9	109.7	132 (4)	120 (2)	126 (3)	126 (2)
$\tau_{1,2,8,12}$	25.9	21.4	29.2	21 (26)	9 (43)	12 (12)	62 (20)
$\tau_{7,9,14,H}$	171.4	169.4	171.3	6 (41)	0 (47)	48 (19)	48 (22)
$\tau_{3,7,9,14}$	122.9	117.9	119.6	24 (64)	4 (49)	74 (12)	70 (12)
$\tau_{10,3,7,9}$	2.0	2.4	2.5	2 (9)	1 (6)	2 (8)	3 (8)

[a] Ensemble averages obtained at 300 K are reported together with the calculated standard deviations. See Figure 1 for a definition of the reported parameters. [b] Gaussian03 B3LYP/TZ minimum structure. [c] Gaussian03 BLYP/TZ minimum structure. [d] CPMD BLYP/PW/PP minimum structure. [e] Averages and standard deviations obtained from the gas phase QM dynamics. [f] In the Amber MD simulations, all of the covalent bond lengths involving H atoms were kept fixed.

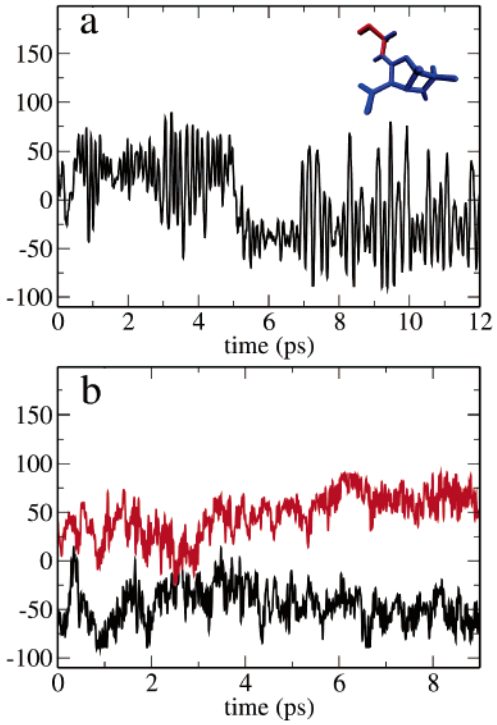

Figure 4. Gas phase (a) and solvated QM (b, black line) and QM/MM (b, red line) instantaneous value (in degrees) for the torsional angle $\tau_{7,9,14,H}$ defining the hydroxymethyl orientation. The torsional angle is evidenced in red in the picture.

TABLE 3: (A) Average Number of H-bonds Formed between Clavulanates' Oxygens and Water and (B) Average Number of Water Molecules Included within the First (within 3.5 Å from the Solute) and Second Solvation Shells (between 3.5 Å and 5.0 Å) for the QM, QM/MM, and Amber Simulations[a]

		QM	QM/MM	Amber
A	O^{12}	2.7 (0.5)	2.8 (0.8)	2.8 (0.6)
	O^{13}	2.0 (0.6)	3.2 (0.8)	2.8 (0.6)
	O^{10}	0.3 (0.4)	0.6 (0.6)	0.7 (0.6)
	O^{11}	1.1 (0.6)	1.4 (0.8)	1.8 (0.7)
	O^{14}	1.8 (0.5)	2.0 (0.6)	1.4 (0.7)
B	first shell	24.9 (2.1)	28.3 (2.0)	23.2 (2.6)
	second shell	45.5 (1.9)	55.2 (3.0)	50.6 (2.9)

[a] The oxygen numbering is given in Figure 1.

though the QM/MM description allows a higher mobility to the group and it takes a longer time to converge to an average value. It is worth noticing that the C−O bond distances of the carboxylate group and the O−H distance ($r_{14,H}$) of the hydroxymethyl are elongated in both the QM and QM/MM simulation for solvated clavulanate with respect to the gas phase. This is an indication of the presence of strong hydrogen bonds between these two groups and the surrounding water.

There are five water molecules forming hydrogen bonds with the two oxygens of carboxylate and two with the oxygen of the hydroxymethyl group (Figure 1b). Two of the waters that are hydrogen bonded to the carboxylate and to the hydroxymethyl are also hydrogen bonded to each other, and this is probably affecting the dynamics of the torsional modes of the two floppy groups in solution. As can be see from Table 3, the QM and the QM/MM simulations predict a similar number of water molecules in the first solvation shell [25 (2) and 28 (2), respectively], while the number of waters in the second solvation shell is slightly different for the two methods [45 (2) and 55 (3), respectively]. The difference in the average number of water molecules in the first shell lies within the calculated standard deviations for all of the three methods employed, whereas for the water molecules in the second solvation shell the result obtained with the QM simulation differs by less than the 10% from that obtained with the QM/MM and the classical simulations. To understand whether the apparent overcoordination provided by the QM/MM method was either due to the differences between the QM and the QM/MM methods or to size effects due to the different dimension of the boxes that were employed, we performed an additional constant volume classical 100 ps-long simulation using the Amber force field starting from the last frame of our QM simulation. The average number of water molecules present in the first and second solvation shells turned out to be 22 (2) and 45 (1), respectively, which is very similar to the average values obtained from the QM simulation [25 (2) and 45 (2), respectively]. Thus, the discrepancies between the QM and the QM/MM simulations can be ascribed to the different size of the box used in the two simulations. However, as will be discussed in the ensuing paragraph, this size effect does not appreciably influence the vibrational properties of clavulanate, being that the QM and the QM/MM results are in good agreement.

The average number of H-bonds (Table 5) and the calculated radial distribution functions (Figure 5) confirm the presence of strong hydrogen bonds between the two oxygens of the carboxylate group (O^{12}, O^{13}) and the oxygen belonging to the hydroxyl group (O^{14}) with water. The two carboxylate oxygens are differently bound to water: from the QM simulation, we calculate 3.2 and 2.8 water molecules bound on average to O^{12} and O^{13}, respectively; this number is slightly lower for the QM/MM simulation (2.6 and 2.3, respectively). The smaller coordination numbers provided by the QM/MM calculation may be related to the higher diffusion constant predicted by the TIP3P water[58] employed in the QM/MM simulation as compared to that predicted by the BLYP density functional.[59] The slight asymmetry for the two oxygens is probably due to a different steric overlap between the carboxylate oxygens (O^{12} and O^{13}) and the rigid frame of clavulanate (Figure 1b). The hydroxymethyl group (O^{14}) is calculated to be bound on average to two water molecules; less significant H-bonds are expected to be formed between the carbonyl oxygen (O^{11}) and water, and very weak hydrogen bonds, if any, are predicted for the ether oxygen (O^{10}) in the ring. This is confirmed from the calculated radial distribution functions (Figure 5). In fact, in both O^{12} and O^{13}, an intense peak at 2.7 Å is observed, indicating the presence of a strong hydrogen bond between the two oxygens and water. This is similarly observed for O^{14}, whereas a broader structure is calculated for O^{11}, and no peak is observed at all for O^{10}. Overall, although the sizes of the boxes are different, the QM and QM/MM simulations qualitatively agree in the description of the solvation structure of clavulanate.

3.2. Vibrational Analysis. The influence of solvation on the vibrational modes of clavulanate was analyzed using the vibrational density of states (VDOS) obtained from the Fourier transform of the atomic velocity autocorrelation function of the gas phase, the QM, and the QM/MM simulations. The Fourier transform was calculated using the Maximum Entropy (all-poles) Method (MEM).[60] The results were compared with the customary fast Fourier transform method and harmonic vibrational analysis on the equilibrium gas phase clavulanate structure. The number of poles used in the MEM was large enough to resolve as much as possible the various spectral features and to provide a stable power spectrum. To test the accuracy due to the phase space sampling, we split the whole QM trajectory in equispaced

TABLE 4: Vibrational Analysis of Clavulanate[a]

	B3LYP/TZ		BLYP/TZ								
mode	ω	$I_\perp$	ω	$I_\perp$	B3LYP/DZ Δ anharmonicity	BLYP/PW	QM vacuo	QM solution	QM/MM solution	exptl[b]	assignment
ν_{13}	415	4	400	4	−10	403			425	424	
ν_{14}	466	7	447	14	−8	483			500	494	
ν_{15}	494	2	468	2	−8	510					
ν_{16}	543	2	519	2	−9	568					
ν_{17}	588	10	558	23	−11	601			610	656	
ν_{18}	655	4	617	6	−12	618					
ν_{19}	667	4	640	4	−12	645					
ν_{20}	704	2	667	3	−11	672					
ν_{21}	746	9	714	9	−14	725			705	742	
ν_{22}	794	2	744	23	−21	760			787	790	
ν_{23}	801	3	760	7	−16	785					
ν_{24}	856	5	796	30	−20	818			849	852	
ν_{25}	869	23	816	13	−30	827					
ν_{26}	896	3	843	3	−18	840					
ν_{27}	913	6	867	5	−18	866				900	
ν_{28}	972	15	894	35	−21	875			988	946	
ν_{29}	987	7	935	3	−18	938					
ν_{30}	1000	13	954	19	−29	969			1066	1100	
ν_{31}	1025	1	975	4	−23	982					
ν_{32}	1044	6	985	8	−31	992				1058	
ν_{33}	1068	3	1020	8	−30	1027					
ν_{34}	1118	5	1058	6	−31	1063					
ν_{35}	1127	7	1082	20	−33	1096			1173	1123	
ν_{36}	1158	29	1100	72	−29	1115					
ν_{37}	1178	13	1130	15	−32	1151					
ν_{38}	1205	10	1150	19	−32	1165			1273	1207	
ν_{39}	1209	0	1162	1	−32	1172					
ν_{40}	1233	11	1192	27	−32	1234					
ν_{41}	1269	22	1226	40	−34	1243					
ν_{42}	1296	13	1243	16	−29	1255	1189	1232	1234	1288	asymmetric $-C^8O_2$ stretch
ν_{43}	1314	12	1250	11	−33	1259					
ν_{44}	1333	8	1276	13	−37	1282					
ν_{45}	1350	10	1287	16	−38	1295					
ν_{46}	1380	6	1330	10	−34	1339					
ν_{47}	1441	9	1389	16	−38	1368	1274	1310	1298		$C^4-H + CH_2-OH$ bend
ν_{48}	1446	10	1410	19	−40	1401	1368	1360	1378	1398	lactam ring C^5H_2 bend
ν_{49}	1515	8	1472	9	−38	1463	1410	1424	1433	1470	C^9H_2 bend
ν_{50}	1733	1166	1653	1318	−43	1637	1566	1586	1575	1699	$C^3=C^7$ stretch
ν_{51}	1744	48	1674	11	−28	1652	1574	1498	1492		symmetric $-C^8O_2$ stretch
ν_{52}	1836	14	1754	16	−38	1743	1635	1666	1673	1780	lactam ring C=O stretch
ν_{53}	2947	266	2865	346	−167	2932	2724	2739	2729		symmetric C^9H_2 stretch
ν_{54}	3034	50	2954	54	−134	2990	2750	2730	2754		asymmetric C^9H_2 stretch
ν_{55}	3066	225	2983	309	−144	2991	2804	2804	2806		symmetric C^5H_2 stretch
ν_{56}	3109	117	3022	140	−155	3032	2851	2898	2910		C^4-H stretch
ν_{57}	3128	83	3045	90	−152	3051	2859	2831	2839		asymmetric C^5H_2 stretch
ν_{58}	3130	69	3052	72	−161	3052	2869	2865	2855		C^2-H stretch
ν_{59}	3188	63	3110	70	−146	2903	2910	3000	2915		C^7-H stretch
ν_{60}	3803	538	3632	1310	−182	3542	3498				O−H stretch

[a] For the B3LYP and BLYP calculations in a Gaussian triple-ζ basis set (B3LYP/TZ and BLYP/TZ), both the harmonic vibrational frequency (cm^{-1}) and the Raman scattering activity ($Å^4$/amu) is reported (see text); for the BLYP calculation in a plane wave basis set and pseudopotentials (BLYP/PW), only the harmonic frequencies (cm^{-1}) are given; the anharmonic correction to the vibrational frequencies calculated with B3LYP and a double-ζ is also reported (Δ anharmonicity (cm^{-1})). The data reported in the three columns labeled with QM and QM/MM refer to the QM and QM/MM simulations at 300 K. Vibrational modes assigned to experimental Raman bands are reported in bold. [b] Reference 63.

time intervals of length ranging from 1.5 to 5 ps and calculated the corresponding frequency of different stretching modes (data not shown). Medium range frequency modes, such as the lactam C=O and the carboxyl C−O bonds, are affected roughly by a 20 cm^{-1} statistical error.

The total VDOS for clavulanate is reported in Figure 6. The different profiles of the total VDOS of clavulanate calculated in the gas phase and in solution are suggestive of a significant influence of solvation. Many of the frequencies observed in the gas phase are largely shifted. QM and QM/MM simulations seem able to provide a similar vibrational spectrum, with slight frequency shifts observed at about 1100 and 1250 cm^{-1}. Not much more information can be obtained from the global VDOS due to the overlap of the various peaks. From an inspection of the VDOS partitioned for the various atomic species, reported in Figure 7, we can observe that the global vibrational profiles

TABLE 5: Normalized Raman Intensities of the Vibrational Modes Assigned to the Experimental and Calculated Bands[a]

mode		B3LYP/TZ	QM/MM	exptl[b]
ν_{42}	asymmetric $-C^8O_2$ stretch	0.10	0.9	0.6
ν_{48}	lactam ring C^5H_2 bend	0.07	0.5	0.8
ν_{49}	C^9H_2 bend	0.06	0.3	0.1
ν_{50}	$C^3{=}C^7$ stretch	1.00	1.0	1.0
ν_{52}	lactam ring C=O stretch	0.08	0.1	0.5

[a] Third column: Gaussian B3LYP/TZ intensities calculated with eq 5. Fourth column: integrated BLYP QM/MM intensity. Fifth column: experimental integrated intensity. All of the intensities are normalized to the $C^{(3)}{=}C^{(7)}$ stretch. [b] Reference 63.

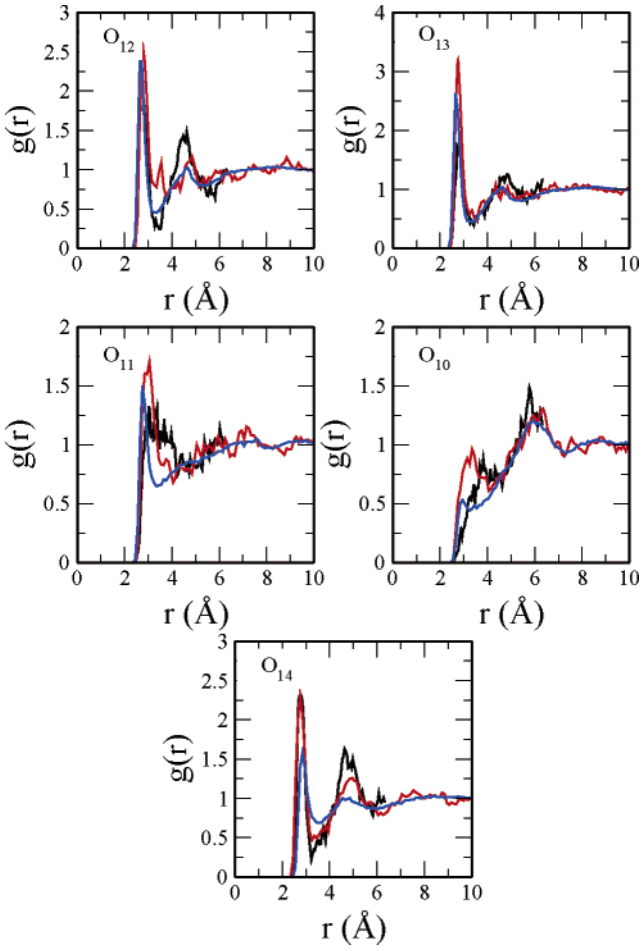

Figure 5. Radial distribution function $g(r)$ for the distance between the oxygens of clavulanate and water (expressed in Å) obtained with the QM (black lines), the QM/MM method (red lines), and the classical simulations (blue lines).

calculated at the QM and QM/MM levels are again in fairly good agreement. The only significant changes are the frequency and intensity shift observed for the O atoms at about 700 cm^{-1}, as one could expect from the different description of the H-bond interactions present in the two models. Despite these slight changes, though, the QM/MM calculation seems to reliably predict the VDOS calculated by the more computationally expensive QM simulation.

In order to perform a quantitative assignment of the vibrational spectrum, the VDOS was projected along the harmonic vibrational normal modes calculated for the equilibrium structure in vacuum (Figure 8). Many normal modes do not appreciably lose their character as a consequence of the thermal motion and solvation effects, giving rise to the sharp single peak spectral features. Instead, some normal modes are "mixed up'' passing from the gas phase to the solution. This is the case of largely

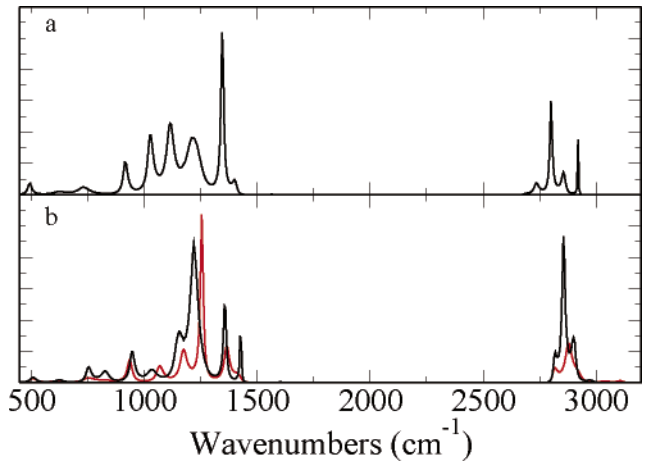

Figure 6. Gas phase (a), and solvated QM/MM (b, red line) and QM (b, black line) vibrational density of states for clavulanate.

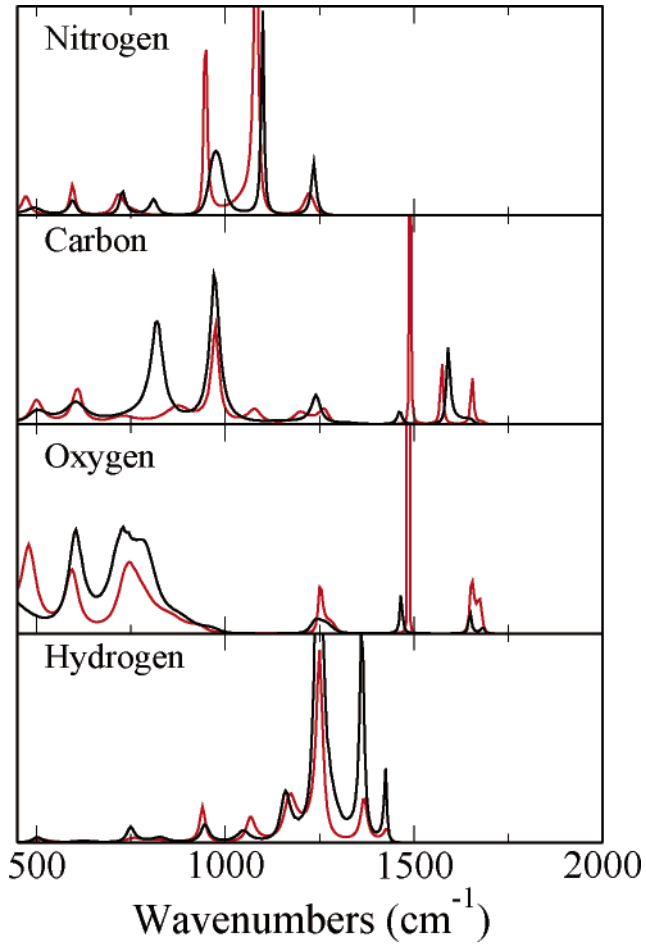

Figure 7. QM (black lines) and QM/MM (red lines) vibrational density of states for clavulanate partitioned for the various atoms types. Intensity in arbitrary units.

delocalized (ω < 1200 cm^{-1}) and very close in frequency normal modes. The vibrational analysis on the finite temperature gas phase simulation suggests that the mixing is largely due to anharmonic effects. We also remark that the character of the normal modes depends to some extent on the level of theory used for the calculation. The dependence is stronger for delocalized modes. Finally, several normal modes lose their identity because of the flexibility of some parts of the molecule. These issues make it extremely difficult to assign low frequency modes. Therefore, we focus on higher frequency modes, which

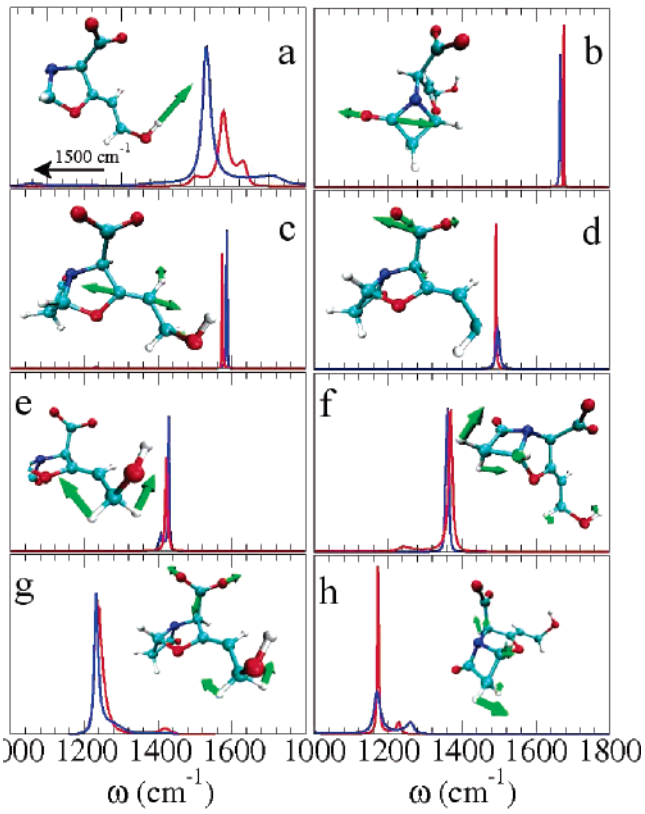

Figure 8. QM/MM (red lines) and QM (blue lines) vibrational density of states projected along the harmonic vibrational normal modes calculated for the equilibrium structure in vacuum at the BLYP level with a plane wave basis set and pseudopotentials. In each frame, the corresponding normal mode is shown with green arrows (only atomic components larger than 0.08 are reported). (a) O−H stretch. (b) Lactam ring C═O stretch. (c) C═C stretch. (d) $-CO_2$ symmetric stretch. (e) Hydroxy methyl $H-C^9-H$ bending. (f) Lactam ring $H-C^5-H_2$ bending. (g) $-CO_2$ asymmetric stretching (this gas phase normal mode has also a contribution from the $H-C^9-H$ bending, which is also clearly visible the power spectrum). (h) This gas phase normal mode involves several C−H bendings, and when it is used as projection vector, it gives rise to two well resolved vibrational frequencies. Intensity in arbitrary units.

are also the most interesting for the understanding of the inhibitor/lactamase binding mechanism.

The majority of the projected QM and QM/MM power spectra in the range between 1000 and 3000 cm^{-1} agrees fairly well. The largest differences are found for the O−H stretch (Figure 8a). This mode gives rise in both simulations to a broad structured band, which largely differs in the two cases, probably because of sampling problems and the very different description of the solute−solvent H-bonding.

The projection procedure allows us to unambiguously assign several important vibrational modes (Table 4). Our calculations show that the BLYP functional underestimates the vibrational frequencies with respect to B3LYP. As expected, anharmonicity shifts down all of the vibrational frequencies (Table 4, column 6). This is also indicated by the finite temperature vibrational analysis of the trajectory of clavulanate in vacuum (Table 4, column 8). In the (classical nuclei) MD trajectory, the downshift is generally larger than the one predicted by the cubic and quartic terms of the nuclear potential energy surface expansion. Solvation affects the various vibrational modes in different, even opposite, ways. For instance, as a consequence of the formation of strong hydrogen-bonds, the frequency of the symmetric $-CO_2$ stretch is red-shifted by roughly 70 cm^{-1}, whereas the asymmetric $-CO_2$ stretch is blue-shifted by about 40 cm^{-1}. The β-lactam C═O stretch does not seem to be particularly influenced by the solvent even though the carbonyl group is on average hydrogen-bonded to one water molecule. As a whole, solvation can affect the vibrational frequency, even of non-solvent hydrogen-bonded residues, by several tens of wavenumbers.

In summary, QM and QM/MM simulations seem to predict vibrational properties in fairly good agreement. This is a non-trivial outcome because the two calculations not only differ in the description of the solute−solvent interactions, but also have been performed on systems with different number of atoms. This suggests that the size effect has only a marginal role.

3.3. Raman Spectrum for Clavulanate in Solution. In this section, the calculated Raman spectrum of clavulanate in aqueous solution will be discussed and an interpretation of the main features of the experimental spectrum will be given. We recall that the Raman spectrum of solvated clavulanate has been previously recorded to help assign the difference Raman spectrum of the inhibitor bound to the E166A SHV-1 β-lactamase active site, while the inhibition reaction was proceeding.[61,62] Difference Raman spectra were obtained by subtracting from the recorded spectrum of the inhibitor bound to the protein that of the protein alone. The assignment of some of the spectral features observed in the difference spectra was crucial to compare the inhibition mechanism of clavulanate to that of the other inhibitors sulbactam and tazobactam and help rationalize their different inhibition capabilities. The absence of a peak from the difference spectra is interpreted as an inhibitor major structural change during the enzymatic reaction.

The Raman spectrum for clavulanate in solution obtained from the QM/MM simulation is shown in Figure 9, together with the spectrum calculated from the B3LYP and BLYP harmonic wavenumbers, which have been corrected with the B3LYP/cc-pVDZ anharmonic constants, and the experimental spectrum taken from ref 63. In Figure 9, the Raman spectrum calculated from the average QM structure including the closest water molecules forming hydrogen bonds with clavulanate (Figure 1b) has also been reported.

Experimentally, the spectral region of interest is the one below 2000 cm^{-1}. It is well known that this region, commonly called the "fingerprint region'', contains many peaks of varying intensities, many of which are not readily identifiable. A key spectral feature observed in the solvated clavulanate Raman spectrum is the peak at 1780 cm^{-1} assigned to the stretch of the C═O bond present in the β-lactam ring, which opens up upon binding to the enzyme.[61,62] Our calculations support this assignment. The strongest peak in this spectral region, at 1699 cm^{-1}, is assigned to the C═C (C^3-C^7) stretch. This double bond is also affected by a conformational change during the inhibition mechanism, due to the opening of the 5-member ring, which leads to the formation of an enamine intermediate during a following step of the proposed reaction mechanism.[61,62] It is interesting to notice that according to both the BLYP and the B3LYP gas phase anharmonic calculations the peak at 1699 cm^{-1}, when compared to the other spectral features observed in this region, is much stronger than the corresponding transition obtained from the QM/MM simulations (see also Table 5). From a comparison of the spectrum calculated in the gas phase with that obtained including the closest water molecules forming hydrogen bonds with clavulanate at the same geometry (see Figure 1b and Figure 9e), it can be seen that solvation, although not significantly affecting the position of the peak, seems to be responsible for its lower intensity with respect to the gas phase calculations. The same transition in the QM/MM simulation is

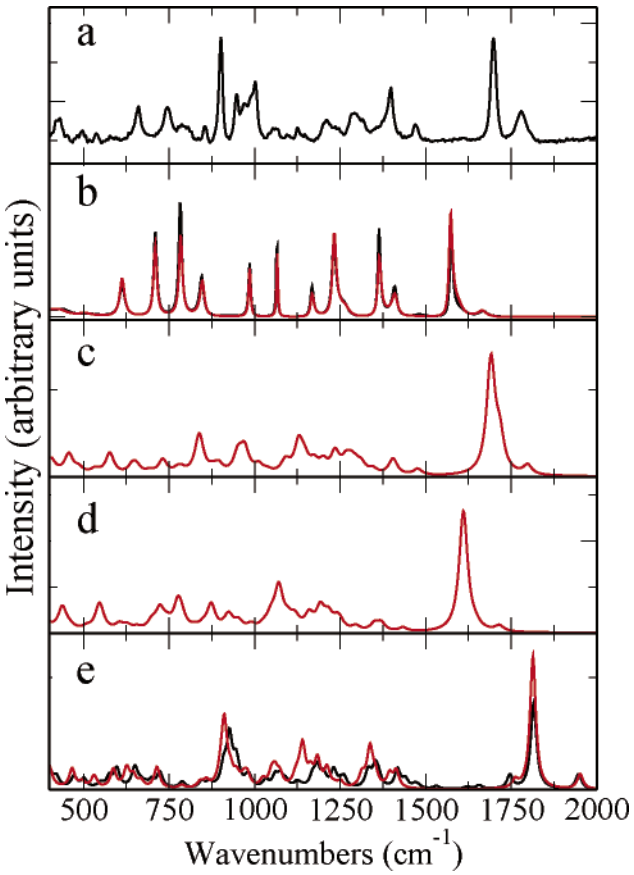

Figure 9. Experimental (a) and calculated (b−e) Raman spectra for clavulanate. (b) Spectra obtained from the B3LYP (red) and BLYP (black) polarizability calculated on the QM/MM trajectory. (c) Gas phase B3LYP/cc-pVTZ harmonic fundamentals and intensities corrected with the B3LYP/cc-pVDZ quartic anharmonic constants. (d) Gas phase BLYP/cc-pVTZ harmonic fundamentals and intensities corrected with the B3LYP/cc-pVDZ quartic anharmonic constants. (e) Comparison between the B3LYP/cc-pVDZ harmonics for the gas phase and microsolvated clavulanate. The gas phase spectra have been obtained summing up Lorentzian functions centered to the harmonic or anharmonic frequencies with a half-height width of 10 cm^{-1} and an area equal to the calculated Gaussian03 Raman intensity (Table 4).

predicted to be of comparable intensity with respect to the various other spectral features that are present at lower wavenumbers (Table 5). We can employ these well characterized and strong peaks at 1780 and 1699 cm^{-1} to establish the accuracy expected with the various models used in this work. The gas phase B3LYP anharmonic calculation predicts them at 1798 and 1691 cm^{-1}, the gas phase BLYP anharmonic calculation at 1714 and 1646 cm^{-1}, and the QM/MM calculation at 1672 and 1575 cm^{-1}, respectively. As already mentioned before, we notice that the BLYP density functional underestimates the calculated frequencies with respect to the B3LYP and that solvation tends to diminish even further the calculated values. Even though the frequencies obtained from the QM/MM simulations are not as accurate as those predicted by the gas phase B3LYP functional, the spectrum predicted by the QM/MM calculation seems to better reproduce the relative intensities of the peaks observed between 400 and 2000 cm^{-1} (Figure 9 and Table 5). The assignment of the peaks observed at lower frequencies is made rather difficult by the fact that in this spectral region most of the vibrational modes are highly delocalized among different regions of the molecule. Nevertheless, several spectral features calculated from the QM/MM simulations can be assigned comparing the calculated spectrum to the VDOS projected along the harmonic vibrational normal modes calculated for the equilibrium structure in vacuum, as discussed in the previous section (Table 4). It is then interesting to notice that the peak at about 1400 cm^{-1} in the experimental Raman spectrum is assigned in ref 62 to the symmetric CO_2 stretch. Its absence from the difference spectrum of clavulanate is interpreted as a further support to the evidence that CO_2 had detached from the inhibitor when the Raman spectrum was recorded. From our QM/MM simulations, the strongest peak in that region, at about 1360 cm^{-1}, is assigned to a delocalized vibration whose major contribution is given by the bending of the lactam ring $H-C^4-H$ group. The symmetric stretch of the CO_2 group is predicted to be at a lower frequency (1262 cm^{-1}) with a lower Raman intensity. Thus, the absence in the difference spectrum of the peak at 1400 cm^{-1} could not be directly related to the decarboxylation of the inhibitor, even though the decarboxylation of clavulanate is experimentally supported;[62] the absence of the peak could be related to the strong interaction between the carboxylate and Arg244 predicted in the preacylation complex.[64]

Other peaks observed in the higher frequency region of experimental spectra can also be unambiguously assigned to the C^9H_2 bending (calculated peak frequency $\approx$ 1433 cm^{-1}; experimental = 1470 cm^{-1}) and to the β-lactam ring C^5H_2 bending (QM/MM calculated peak frequency $\approx$ 1378 cm^{-1}; experimental = 1398 cm^{-1}). The other spectral features present in the Raman spectrum are due to highly delocalized vibrational motions and hence cannot be easily assigned. Therefore, for the remaining bands at lower frequency, only a tentative assignment based on frequency correspondence and spectral shape similarity was done and reported in Table 4.

4. Conclusions

The molecular structure and the vibrational spectrum for clavulanate in the gas phase and in solution have been studied by means of QM and QM/MM simulations. Solvation affects particularly the floppiest parts of the molecule, that is the torsion of the carboxylate and of the hydroxymethyl groups. The three oxygens belonging to these groups are responsible for the strongest hydrogen bonds of clavulanate with water. The dynamical evolution of both the carboxylate and the hydroxymethyl groups differs in the three different type of simulations, probably as a consequence of the different description of the hydrogen bonding, size effects, and sampling problems. Nevertheless, from the clavulanate vibrational density of states it can be seen that both the QM and QM/MM simulations are able to describe the most relevant spectral features present in the interval 1000−2000 cm^{-1}. Raman spectroscopy can be proficiently employed to study solvated systems in that spectral region thanks to the small contribution of water to the total Raman cross section. We have calculated the Raman spectrum of clavulanate in solution assuming that the polarizability of the whole system can be approximated to that of the solute electrostatically interacting with the surrounding water molecules. No significant differences have been observed when calculating the polarizability tensor along the BLYP QM/MM trajectory employing either the BLYP or the B3LYP density functionals. In our calculations, we have neglected dipole−induced dipole interactions involving water, which have been recently suggested to play a role for ionic systems.[65,66] In this regard, we remark that the use of a simple nonpolarizable force field for the solvent seemed to be adequate for the purpose of a comparison of the Raman spectrum to experiment and for the assignment of the most important spectral lines. We also remark that nuclear quantum effects, which can affect both the

frequency and the intensity of the spectral transitions,[67] have not been taken into account in our calculations. Nevertheless, this model has allowed us to calculate the Raman spectrum for solvated clavulanate more realistically than with accurate gas phase anharmonic models. In particular, the relative intensities for the various spectral features appearing in the Raman spectrum seem to be more reliably predicted by the QM/MM simulation when compared to the spectra calculated from the derivatives of the polarizability tensor with respect to the molecular normal modes at equilibrium;[45] this is probably due to the solvent electrostatic field and large amplitude internal degree of freedom (expecially those of carboxylate and hydroxymethyl groups), which are not correctly described when treating the molecule as semirigid.

In conclusion, the proposed computational protocol opens up the possibility of employing QM/MM simulations to calculate the Raman spectra for the various stages of the inhibition mechanism of β-lactamases. This will provide a deeper insight to the reaction mechanism by helping to interpret and assign the collected experimental data.

Acknowledgment. The authors acknowledge computational support from INFM and CINECA. Dr. Helfand is supported by a Department of Veterans Affairs Advanced Career Development Award.

References and Notes

(1) Helfand, M. S.; Totir, M. A.; Carey, M. P.; Hujer, A. M.; Bonomo, R. A.; Carey, P. R. *Biochemistry* **2003**, *42*, 13386.
(2) Carey, P. R. *Annu. Rev. Phys. Chem.* **2006**, *57*, 527.
(3) Helfand, M. S.; Berthel, C. R.; Hujer, A. M.; Hujer, K. M.; Anderson, V. E.; Bonomo, R. A. *J. Biol. Chem.* **2003**, *278* (52), 52724.
(4) Zheng, X.; Rivera-Hainaj, R. E.; Zheng, Y.; Pusztai-Carey, M.; Hall, P. R.; Yee, V. C.; Carey, P. R. *Biochemistry* **2002**, *41* (35), 10741.
(5) Padayatti, P. S.; Helfand, M. S.; Totir, M. A.; Carey, M. P.; Carey, P. R.; Bonomo, R. A.; van den Akker, F. *Biochemistry* **2004**, *43*, 843.
(6) Bonomo, R. A.; Rice, L. B. *Front. Biosci.* **1999**, *4*, e34.
(7) Polyansky, O. L.; Császár, A. G.; Shirin, S. V.; Zobov, N. F.; Barletta, P.; Tennyson, J. *Science* **2003**, *299*, 539.
(8) Rajamäki, T.; Miani, A.; Halonen, L. *J. Chem. Phys.* **2003**, 118, 10929.
(9) Barone, V. *J. Chem. Phys.* **2005**, *122*, 014108.
(10) Boese, A. D.; Klopper, W.; Martin, J. M. L. *Int. J. Quantum Chem.* **2005**, *104*, 830.
(11) Miani, A.; Cané, E.; Palmieri, P.; Trombetti, A.; Handy, N. C. *J. Chem. Phys.* **2000**, *112*, 248.
(12) Car, R.; Parrinello, M. *Phys. Rev. Lett.* **1985**, *55* (22), 2471.
(13) Marx, D.; Hutter, J. In *Modern Methods and Algorithms of Quantum Chemistry*; Grotendorst, J., Ed.; Forschungzentrum Jülich: Jülich, Germany, 2000; Vol. 1, p 301.
(14) Zhu, Z. W.; Tuckerman, M. E. *J. Phys. Chem. B* **2002**, *106*, 8009.
(15) Rousseau, R.; Kleinschmidt, V.; Schmitt, U. W.; Marx, D. *Phys. Chem. Chem. Phys.* **2004**, *6*, 1848.
(16) Gaigeot, M. P.; Sprik, M. *J. Phys. Chem. B* **2003**, *107*, 10344.
(17) Gaigeot, M. P.; Sprik, M. *J. Phys. Chem. B* **2004**, *108*, 7458.
(18) Gaigeot, M. P.; Vuilleumier, R.; Sprik, M.; Borgis, D. *J. Chem. Theory Comput.* **2005**, *1*, 772.
(19) Klahn, M.; Schlitter, J.; Gerwert, K. *Biophys. J.* **2005**, *88*, 3829.
(20) Putrino, A.; Sebastiani, D.; Parrinello, M. *J. Chem. Phys.* **2000**, *113* (17), 7102.
(21) Putrino, A.; Parrinello, M. *Phys. Rev. Lett.* **2002**, *87* (17), 176401−1.
(22) Nonella, M.; Mathias, G.; Tavan, P. *J. Phys. Chem. A* **2003**, *107*, 8638.
(23) Klähn, M.; Mathias, G.; Kötting, C.; Nonella, M.; Schlitter, J.; Gerwert, K.; Tavan, P. *J. Phys. Chem. A* **2004**, *108*, 6186.
(24) Kinnaman, C. S.; Cremeens, M. E.; Romesberg, F. E.; Corcelli, S. A. *J. Am. Chem. Soc.* **2006**, *128*, 13334.
(25) Cui, Q.; Karplus, M. *J. Chem. Phys.* **2000**, *112* (3), 1133.
(26) Schmitz, M.; Tavan, P. *J. Chem. Phys.* **2004**, *121*, 12233.
(27) Schmitz, M.; Tavan, P. *J. Chem. Phys.* **2004**, *121* (24), 12247.
(28) Laio, A.; VandeVondele, J.; Rothlisberger, U. *J. Chem. Phys.* **2002**, *116* (16), 6941.
(29) Laio, A.; VandeVondele, J.; Rothlisberger, U. *J. Phys. Chem. B* **2002**, *106*, 7300.
(30) Lazzeri, M.; Mauri, F. *Phys. Rev. Lett.* **2003**, *90*, 036401.
(31) Wirtz, L.; Lazzeri, M.; Mauri, F.; Rubio, A. *Phys. Rev. B* **2005**, *71*, 241402.
(32) Jorgensen, W. L.; Chandrasekhar, J.; Madura, J.; Klein, M. L. *J. Chem. Phys.* **1983**, *79*, 926.
(33) Case, D.; Cheatham, T.; Darden, T.; Gohlke, H.; Luo, R.; Merz, K.; Onufriev, A.; Simmerling, C.; Wang, B.; Woods, R. *J. Comput. Chem.* **2005**, *26*, 1668.
(34) Wang, J.; Wolf, R. M.; Caldwell, J. W.; Kollman, P. A.; Case, D. A. *J. Comput. Chem.* **2004**, *25*, 1157.
(35) Wang, J.; Wang, W.; Kollman, P. A.; Case, D. A. *J. Mol. Graphics Modell.* **2006**, *25*, 247260.
(36) Grest, G. S.; Kremer, K. *Phys. Rev. A* **1986**, *33* (5), 3628−3631.
(37) Becke, A. D. *Phys. Rev. A* **1988**, *38*, 3098.
(38) Lee, C.; Yang, W.; Parr, R. *Phys. Rev. B* **1988**, *37*, 785.
(39) Troullier, N.; Martins, J. L. *Phys. Rev. B* **1991**, *43*, 1993.
(40) Sprik, M.; Hutter, J.; Parrinello, M. *J. Chem. Phys.* **1996**, *105*, 1142.
(41) Neilson, D., Das, M. P., Eds.; *Computational Approaches to Novel Condensed Matter Systems*, Proceedings of 3rd Gordon Godfrey Workshop on Condensed Physics; Plenum: New York, 1995.
(42) Hutter, J.; Alavi, A.; Deutch, T.; Bernasconi, M.; Goedecker, S.; Marx, D.; Tuckerman, M.; Parrinello, M. *Cpmd Technical report*; MPI für Festkörperforschung and IBM Zurich Research Laboratory: 1995−1999.
(43) Wang, J.; Cieplak, P.; Kollman, P. A. *J. Comput. Chem.* **2000**, *21*, 1049.
(44) Tuckerman, M.; Martyna, G. J.; Klein, M. L. *J. Chem. Phys.* **1992**, *97*, 2635.
(45) Frisch, M. J.; Trucks, G. W.; Schlegel, H. B.; Scuseria, G. E.; Robb, M. A.; Cheeseman, J. R.; Montgomery, J. A., Jr.; Vreven, T.; Kudin, K. N.; Burant, J. C.; Millam, J. M.; Iyengar, S. S.; Tomasi, J.; Barone, V.; Mennucci, B.; Cossi, M.; Scalmani, G.; Rega, N.; Petersson, G. A.; Nakatsuji, H.; Hada, M.; Ehara, M.; Toyota, K.; Fukuda, R.; Hasegawa, J.; Ishida, M.; Nakajima, T.; Honda, Y.; Kitao, O.; Nakai, H.; Klene, M.; Li, X.; Knox, J. E.; Hratchian, H. P.; Cross, J. B.; Bakken, V.; Adamo, C.; Jaramillo, J.; Gomperts, R.; Stratmann, R. E.; Yazyev, O.; Austin, A. J.; Cammi, R.; Pomelli, C.; Ochterski, J. W.; Ayala, P. Y.; Morokuma, K.; Voth, G. A.; Salvador, P.; Dannenberg, J. J.; Zakrzewski, V. G.; Dapprich, S.; Daniels, A. D.; Strain, M. C.; Farkas, O.; Malick, D. K.; Rabuck, A. D.; Raghavachari, K.; Foresman, J. B.; Ortiz, J. V.; Cui, Q.; Baboul, A. G.; Clifford, S.; Cioslowski, J.; Stefanov, B. B.; Liu, G.; Liashenko, A.; Piskorz, P.; Komaromi, I.; Martin, R. L.; Fox, D. J.; Keith, T.; Al-Laham, M. A.; Peng, C. Y.; Nanayakkara, A.; Challacombe, M.; Gill, P. M. W.; Johnson, B.; Chen, W.; Wong, M. W.; Gonzalez, C.; Pople, J. A. *Gaussian 03*, revision C.02; Gaussian, Inc.: Wallingford, CT, 2004.
(46) Barnett, R. N.; Landman, U. *Phys. Rev. B* **1993**, *48*, 2081.
(47) Becke, A. *J. Chem. Phys.* **1993**, *98*, 5648.
(48) Dunning, T. H., Jr. *J. Chem. Phys.* **1989**, *90*, 1007.
(49) Papousek, D.; Aliev, M. R. *Molecular Vibrational-Rotational Spectra;* Elsevier Scientific Publishing Company: Atlanta, GA, 1982.
(50) Bright Wilson, E., Jr.; Decius, J. C.; Cross, P. C. *Molecular Vibrations: the Theory of Infrared and Raman Vibrational Spectra*; Dover Publications, New York, 1980.
(51) Herzberg, G. *Molecular Spectra and Molecular Structure*; Krieger Publishing Company, Melbourne, FL, 1991; Vol. 2.
(52) Porezag, D.; Pederson, M. *Phys. Rev. B* **1996**, *54* (11), 7830.
(53) McQuarrie, D. A. *Statistical Mechanics*; Harper Collins Publisher: New York, 1973.
(54) Gordon, R. G. *J. Chem. Phys.* **1965**, *42*, 3658.
(55) Bader, J. S.; Berne, B. J. *J. Chem. Phys.* **1994**, *100*, 8359.
(56) Hall, G. G.; Smith, C. M. *Int. J. Quantum Chem.* **1984**, *25*, 881.
(57) Smith, C. M.; Hall, G. G. *Theor. Chim. Acta* **1986**, *69*, 63.
(58) Mahoney, M. W.; Jorgensen, W. L. *J. Chem. Phys.* **2001**, *114* (1), 363.
(59) Sprik, M.; Hutter, J.; Parrinello, M. *J. Chem. Phys.* **1996**, *105* (3), 1142.
(60) Press, W. H.; Flannery, B. P.; Teukolsky, S. A.; Vetterling, W. T. *Numerical Recipes: The Art of Scientific Computing*, 2nd ed.; Cambridge University Press: Cambridge, U.K., 1992.
(61) Helfand, M. S.; Totir, M. A.; Carey, M. P.; Hujer, A. M.; Bonomo, R. A.; Carey, P. R. *Biochemistry* **2003**, *42*, 13386.
(62) Padayatti, P. S.; Helfand, M. S.; Totir, M. A.; Carey, M. P.; Carey, P. R.; Bonomo, R. A.; van den Akker, F. *J. Biol. Chem.* **2005**, *280* (41), 34900.
(63) Helfand, M. S.; Berthel, C. R.; Hujer, A. M.; Hujer, K. M.; Anderson, V. E.; Bonomo, R. A. *J. Biol. Chem.* **2003**, *278* (52), 52724.
(64) Imtiaz, U.; Billings, E. M.; Knox, J. R.; Mobashery, S. *Biochemistry* **1994**, *33*, 5728.
(65) Glover, W. J.; Madden, P. A. *J. Chem. Phys.* **2004**, *121*, 7293.
(66) Madden, P. A.; Wilson, M.; Hutchinson, F. *J. Chem. Phys.* **2004**, 120, 6609.
(67) Ramirez, R.; Lopez-Ciudad, T.; Kumar, P.; Marx, D. *J. Chem. Phys.* **2004**, *121*, 3973.